AD-A065 295 MICHIGAN UNIV ANN ARBOR SPACE PHYSICS RESEARCH LAB F/G 22/1
INVESTIGATION OF THE INTERACTION BETWEEN THE S3-2 SATELLITE AND--ETC(U)
OCT 78 U SAMIR, C LAKE F19628-78-C-0046
UNCLASSIFIED AFGL-TR-78-0291 NL

| OF |
AD
A065295

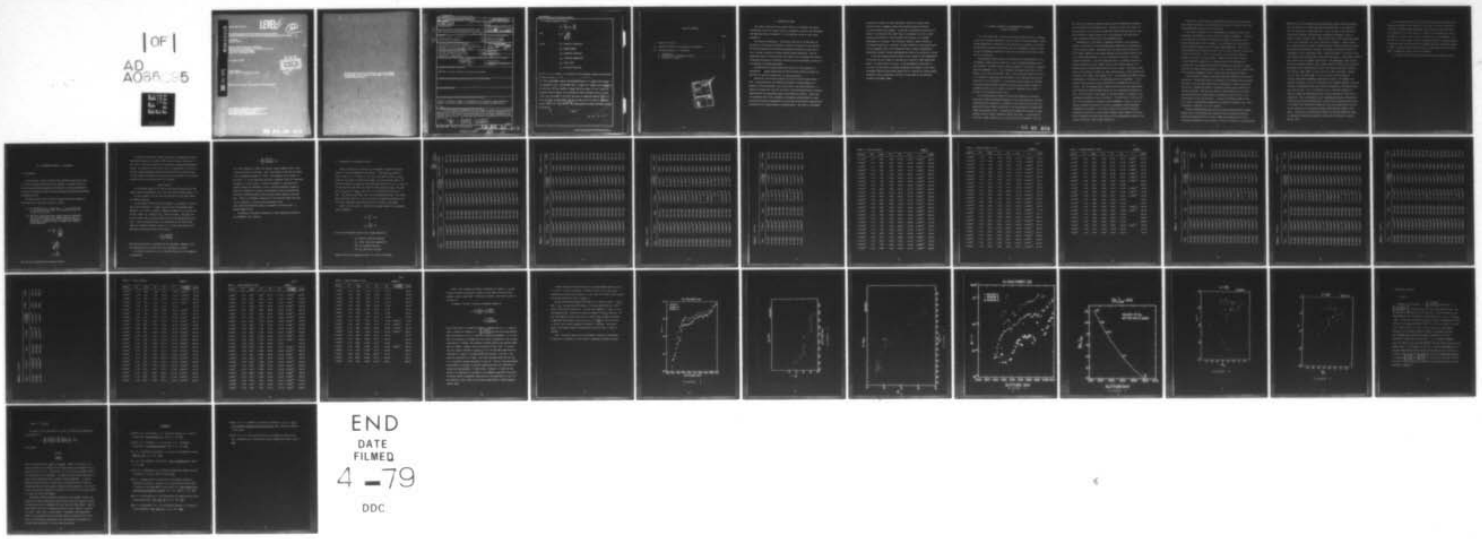

END
DATE
FILMED
4 -79
DDC

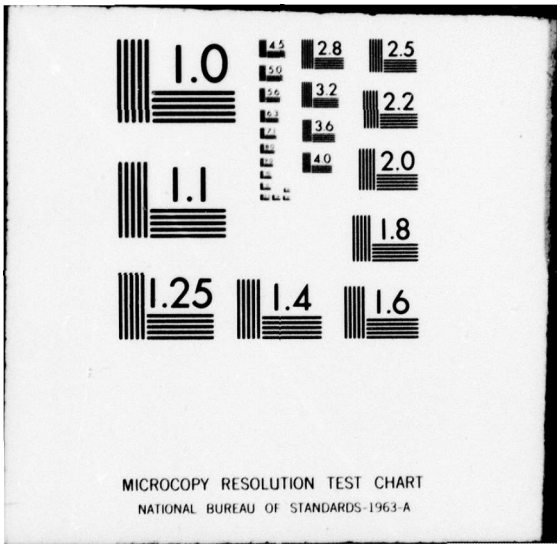
1.0
1.1
1.25
1.4
1.6
1.8
2.0
2.2
2.5
2.8
3.2
3.6
4.0
MICROCOPY RESOLUTION TEST CHART
NATIONAL BUREAU OF STANDARDS-1963-A

LEVEL II

AFGL-TR-78-0291

INVESTIGATION OF THE INTERACTION BETWEEN THE S3-2 SATELLITE AND ITS ENVIRONMENTAL SPACEPLASMA

Uri Samir
Charles Lake

Space Physics Research Laboratory
Department of Atmospheric and Oceanic Science
The University of Michigan
Ann Arbor, Michigan 48109

31 October 1978

Final Report
1 May 1978 - 30 September 1978

AIR FORCE GEOPHYSICS LABORATORY
AIR FORCE SYSTEMS COMMAND
UNITED STATES AIR FORCE
HANSCOM AFB, MASSACHUSETTS 01731

Unclassified

SECURITY CLASSIFICATION OF THIS PAGE (When Data Entered)

REPORT DOCUMENTATION PAGE

READ INSTRUCTIONS BEFORE COMPLETING FORM

1. REPORT NUMBER	2. GOVT ACCESSION NO.	3. RECIPIENT'S CATALOG NUMBER
AFGL-TR-78-0291		

4. TITLE (and Subtitle)

INVESTIGATION OF THE INTERACTION BETWEEN THE S3-2 SATELLITE AND ITS ENVIRONMENTAL SPACEPLASMA.

5. TYPE OF REPORT & PERIOD COVERED

Final Report.
1 May [illegible] - 30 Sep [illegible] 1978.

6. PERFORMING ORG. REPORT NUMBER

7. AUTHOR(s)

Uri Samir, Charles Lake

8. CONTRACT OR GRANT NUMBER(s)

F19628-78-C-0046

9. PERFORMING ORGANIZATION NAME AND ADDRESS

Space Physics Research Laboratory, Dept. of Atmospheric and Oceanic Science, The University of Michigan, Ann Arbor, Michigan 48109

10. PROGRAM ELEMENT, PROJECT, TASK AREA & WORK UNIT NUMBERS

62101F
DMSPOOAB
Proj 7661 Task 7661-06

11. CONTROLLING OFFICE NAME AND ADDRESS

Air Force Geophysics Laboratory
Hanscom AFB, Massachusetts 01731
Monitor/R. C. Sagalyn/PHG

12. REPORT DATE

31 Oct 78

13. NUMBER OF PAGES

42

14. MONITORING AGENCY NAME & ADDRESS (if different from Controlling Office)

43p.

15. SECURITY CLASS. (of this report)

Unclassified

15a. DECLASSIFICATION/DOWNGRADING SCHEDULE

16. DISTRIBUTION STATEMENT (of this Report)

Approved for public release; distribution unlimited.

17. DISTRIBUTION STATEMENT (of the abstract entered in Block 20, if different from Report)

18. SUPPLEMENTARY NOTES

19. KEY WORDS (Continue on reverse side if necessary and identify by block number)

Wake of a satellite, amount of ion depletion in the wake, plasma parameters, plasma oscillations parametric dependence, Shuttle/Spacelab application.

20. ABSTRACT (Continue on reverse side if necessary and identify by block number)

Ion and electron measurements from the planar ion probes and the spherical electron probe onboard the S3-2 satellite were used in order to investigate the distribution of ion current around the satellite in the closest proximity to the surface. In particular, the investigation focussed on examining the variation of the ratios:

next page

$$\alpha = \left[\frac{I_+(\text{wake})}{I_+(\text{front})}\right] \approx \left[\frac{I_+(\text{wake})}{I_+(\text{ambient})}\right]$$

(over)

DD FORM 1 JAN 73 1473 EDITION OF 1 NOV 65 IS OBSOLETE

Unclassified
SECURITY CLASSIFICATION OF THIS PAGE (When Data Entered)

79 03 02 019

328 650

LB

with plasma parameters such as

$$R_D = \frac{R_o}{\lambda_D}; \quad \phi_N = \frac{e\phi_s}{KT_e}$$

and

$$S_{AV} = \frac{V_s}{\sqrt{\frac{2KT_e}{M_+}}}$$

where R_o = radius of satellite

λ_D = Debye length

ϕ_s = satellite potential

T_e = electron temperature

M_+ = ionic mass

V_s = satellite velocity

The ratio α is a measure of the amount of perturbation created by the motion of the satellite.

The preliminary results obtained demonstrate in a quantitative manner the dependence of $\alpha = f(\text{altitude})$ and $\alpha = f(R_D)$ for: $24 < R_D < 56$ and $10 < |\phi_N| < 18$. We find that α at an altitude of about 300 km is about 2.5 to 3 orders of magnitude smaller than α at an altitude of about 500-600 km and α at this latter altitude range is by about one order of magnitude smaller than α at about 1100 km. We also find α for $R_D \cong 54$-56 to be 3.5 order of magnitude smaller than α for $R_D \cong 24$-30. The investigation already performed yielded new results.

TABLE OF CONTENTS

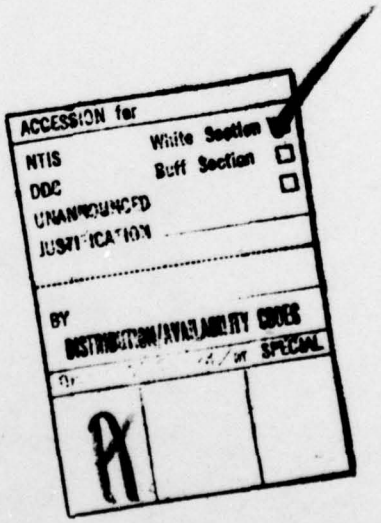

I. OBJECTIVE OF STUDY

The overall objective of the present study is to determine the angular distribution of the ion current around an ionospheric satellite and investigate phenomenologically the dependence of the normalized current on some plasma parameters.

The overall technological - application objective is to determine the extension of the spatial disturbances created by the motion of the satellite and their interaction with thermal measurements performed by plasma probes (e.g., current collectors of various kinds) onboard satellites. From the application point of view the above study should aid in assessing the validity, reliability and quality of particle and field in-situ measurements and help in the planning of Spacelab experiments.

Scientifically the study should yield clues as to the existence or nonexistence of plasma oscillations and shock patterns ahead and behind the satellite for specific combinations of plasma parameters.

Technically, and from the application point of view, the study should have a strong bearing on the planning and design of probe packages to be mounted on future satellites, and in particular on the Shuttle/Spacelab. It should be realized that now with the advent of Shuttle/Spacelab many ionospheric magnetospheric and spaceplasma physics experiments are planned. These types of experiments will utilize ensembles of diagnostic probes mounted on booms ejectable instrument packages (known as throw away detectors) and on maneuverable subsatellites of varying degrees of sophistication. The types of instruments

considered at present for such experiments include low energy current collectors such as Langmuir probes and retarding potential analyzers (of various kinds) and antennas. In the past, perturbations created by the motion of the satellite were never taken too seriously in as far as their potential contribution to the reliability and validity of low energy measurements is concerned. This situation, however, cannot continue in the coming Spacelab era. Therefore, the main objective of the present study and the suggested study of the coming few years is mainly technological/ application oriented, without diminishing the value of the scientific outcome.

In the last contract period we have focused mainly on the investigation of the ratio of ion current, in the wake as a function of some plasma parameters. In other words, we focused on investigating the variations of the ratio of the current in the wake normalized with respect to the current as measured when the probe looked ahead (=α) as a function of various plasma parameters, and in particular, the ratio of the radius of the satellite divided by the Debye length.

II. GENERAL SCIENTIFIC AND TECHNOLOGICAL BACKGROUND - BRIEF DISCUSSION

It is well known that a spacecraft orbiting around the earth or orbiting in any other planetary environment interacts with its space environment thereby causing significant perturbations in the near and far vicinity to its surface. The interaction between the spacecraft and its environmental plasma is mutual in that the phenomena involved are coupled by the effects on the space plasma and on the spacecraft.

The spacecraft itself acquires a potential due to the collection of the surrounding, charged particles, and due to other charging mechanisms, such as: photo-emission, secondary particle emission, magnetic field effects, energetic particle bombardment, etc. (e.g., Whipple, 1965; Samir and Willmore, 1965; Whipple, 1977; Samir and Willmore, 1966). The interaction implies that there is a transfer of charge from the environment to the spacecraft and from the spacecraft to the environment. In stating the above we ignore the transfer of charge between different elements on the spacecraft surface; namely, we assumed the surface to be a perfect conductor. Needless to say, that in practice this is usually not the case.

The surrounding space plasma is strongly perturbed by the satellite motion and a wake zone depleted unequally of ions and electrons is therefore formed behind the spacecraft. In addition to the creation of the wake, the spacecraft excites plasma oscillations in the electrostatic ion plasma mode (Samir and Willmore, 1965). A potential well behind the spacecraft at some distance from its surface downstream should also exist. It can be anticipated (Liu, 1969; Gurevich et al., 1970; Gurevich and Pitaevski, 1975; and

Liu, 1975) that plasma oscillations and/or particle energization mechanisms are associated with the potential well. Moreover, the fact that there is a steep gratient in electron and ion densities between the wake zone and elsewhere around the satellite gives rise to the prediction that some kind of plasma instability should exist in the disturbed zones.

Mathematically, the complex of phenomena involved in the interaction between a spacecraft and its surrounding space plasma has to be described in a self-consistant manner. This means that the Vlasov equation written for each charged component of the plasma together with the Poisson equation have to be solved simultaneously in a self-consistent way subject to realistic boundary conditions. It is well known that this is a difficult task and no general solutions yet exist despite the fact that various aspects of the interaction were studied theoretically for over a decade. For general review papers on the subject we sight Liu, 1969; Gurevich et al., 1970; Gurevich and Pitaevski, 1975; Samir, 1973; Whipple, 1977. The available wake models require confirmation or varification via comparing theory with experiment. At the present time the status of such verification or confirmation is not satisfactory. The few attempts made to compare results from in situ measurements with theoretical sheath and wake models are to be considered preliminary at best. This situation is due largely to the small amount of relevant in situ information available for such an analysis. It should also be realized that the in situ information available is often fragmentary in that not all the physical parameters required to carry out a meaningful theory experiment comparison are available. The present status of the study is therefore exploratory and there is a great need to examine larger samples of electron and ion densities (currents) and potential field measurements relevant to the study of spacecraft space plasma interaction.

There can be little doubt that perturbations created by the interaction have profound relevance to the realiability and quality of particle and field measurements made from satellites and rockets.

The study of available in situ measurements is expected to help in the development and planning of future active and passive experiments. It should be realized that the planning of experiments relevant to spacecraft space plasma interactions is now in progress. The planning aims at utilizing the shuttle spacelab facility as a near earth plasma laboratory. Until now we focussed mainly on the application aspect of our study. However, as mentioned earlier we would like to utilize the results so as to obtain scientific information relevant to future studies. Namely we would like to perform a theory experiment comparison via comparing results from the measured ion depletions in the wake with (as far as possible) the theoretical computations for the similar plasma parameters. Hence, examine the real insignificance of the physical assumptions used in constructing the theoretical models.

A brief general discussion regarding theoretical studies is at this point appropriate. As mentioned earlier the problem of the theoretically calculated structure of the disturbed plasma around a moving body in space involves the solution of a complicated system of coupled non-linear partial differential-integral equations. The equations consist of Vlasov equations for the ions and electrons and the Poisson equation relating the electric field to the distributions of ions and electrons. In cases of stationary bodies as well as in cases of moving bodies combinations of numerical techniques (e.g. finite differences, iterations, etc.) are required.

Various approaches have been used in the past to deal with this problem; however, due to the difficulties involved in the self-consistent solution, simplified assumptions had to be used. Among the customary ones we cite: ignoring the geomagnetic field influence on particle collection, using simplified

geometries for body configuration, using simplified surface reactions, assuming that the satellite is a conducting body, and assuming that it is justified to treat the problem as a steady state one. One of the more recent theoretical studies which adopted a self-consistent mathematical treatment is that of Parker as given in Parker, 1976. Parker adopted some of the simplifying assumptions but has advantages over other theoretical treatments. Parker's method uses a numerical grid (or mesh) of discrete points in space where the potential and density distributions are defined. The Poisson and Vlasov equations are represented in finite difference form at these grid points. In his most recent work, Parker used a pillbox shaped body where the surface of the pillbox coincides with certain rows and columns of grid points. One advantage is that the grid points are unequally spaced so that a higher density of points can be used near the surface and a lower density of points used further away from the surface. This allows a given number of grid points to be used efficiently. Despite the fact that this model seems to us to be the most sophisticated and realistic wake model fundamental questions still exist. For example, the question of whether or not is it justified to use a kinetic approach at certain distances surrounding the body and a fluid-like approach at distances further away from the body. Or is it justified to use a fluid-like approach for specific plasma and body parameters and a kinetic approach for other sets of parameters. This is undoubtedly a very interesting scientific problem which should have far reaching applications in cosmic electro dynamics when interest is focussed on the interaction between the solar wind around planets and the natural satellite and interstellar plasma interacting with bodies in deep space. For details on the difference between the approach adopted by Parker as compared with approaches adopted by other authors reference is given to Parker, 1976.

In the present study we were concerned with one aspect only, namely with examining the amounts of ion depletion in the wake of the S3-2 satellite as a function of several plasma parameters, since we believed that the amount of ion depletion in the wake serves as a measure of the significance of the disturbances created by the motion of the satellite to its environment. We will also (at a later stage) attempt a comparison between the measured amounts of depletion with results obtained from Parker's and other theoretical models in order to achieve the more scientific goal of assessing the relative importance of assumptions used in various wake models.

In the next section we present and discuss some preliminary results.

III. PRELIMINARY RESULTS - A DISCUSSION

1. Introduction

During the last contract period we have focussed on getting the data in a form that lends itself best to our purposes. We should state that we have encountered some unexpected difficulties in the data-handling but we do have now samples of data that were analyzed yielding some interesting perliminary results.

The main research effort focused on extracting selected samples of data from the S3-2 satellite in order to obtain:

(i) the variation of $I_+ = f(\theta)$, where: I_+ = ion current and θ = angle between the normal (to the probe) and the satellite velocity vector

(ii) the basic plasma properties; namely, electron temperature (T_e), electron density (N_e), plasma potential (ϕ_s) (or: potential of the spherical electron probe with respect to the plasma), required in order to compute the following plasma parameters:

$$R_D = \frac{R_o}{\lambda_D} = \frac{R_o}{6.9\sqrt{\frac{T_e}{N_e}}}$$

$$S = \frac{V_s}{\sqrt{\frac{2kT_e}{M_+}}}$$

$$\phi_N = \frac{e\phi_s}{kT_e}$$

Note that M_+ is assessed from ionospheric models.

In addition we devoted a considerable effort to modifying the Parker wake/sheath program (e.g. Parker, 1976) trying to make it applicable to the case of a satellite moving in the terrestrial ionosphere-magnetosphere plasma. The objective of the latter effort is (eventually) to be able to perform a theory-experiment comparison which is after all the best test for the validity of theoretical models and for the validity of the physical assumption used in the construction of the models.

About the Data

At the present stage of the study we have used ion-current data from several selected passes/Orbit 1131, orbit data 2/24/76 using sensors 1 - 8.

As will be seen in the next section the quality of the data differs for different sensors.

At the present time we have plots showing: I_+ (in amps) = f (G.M.T.) and we have the angles: θ, $(\underline{n},\underline{B})$, $(\underline{V_s},\underline{B})$ for the corresponding times. Therefore, we are able to examine a reasonable sample of $I_+ = f(\theta)$ in the altitude range: $H_1 \sim 1100$ km to $H_2 \simeq 300$ km (or less). The quality of the data varies and we encounter difficulties in the perigree part of the orbit. This is unfortunate since the information at the low-altitude range is of greater scientific value to us. On the other hand even the above data yielded upper limits to the ratio:

$$\alpha = \left[\frac{I_+ \text{ (wake)}}{I_+ \text{ (front)}}\right]$$

which are not yet known or published in the literature. Moreover, from the application point of view, the latter information is useful.

It should be realized that at the present time we are not attempting to computerize

$$\alpha = \left[\frac{I_+ \text{ (wake)}}{I_+ \text{ (front)}}\right] = f(\theta)$$

in a 'blind' manner but rather use computer outputs together with a close 'visual inspection' of the data. Due to the quality of the data this seems to us a reasonable procedure to follow. This approach may be altered in the future. It is our experience that such an approach 'pays off' eventually although it is slow in time. It should be possible in principle and if enough resources are available to write a pattern-recognition program to compute $[I_+ \text{ (wake)}]$ but we doubt the usefulness of such an approach when the study is problem-oriented using relatively small samples of selected data. After our preliminary examination of the selected passes from orbit 1131 is completed, we will use more measurements from other orbits and extend the study to utilization of E-field data, i.e. Michael Smiddy's data.

In addition to the above information, we have computed the values of the parameters: R_D, S and ϕ_N.

2. Presentation of Preliminary Results

Table 1 gives the ion currents (I_+) the angles of attack (θ) and the ratios (α) for the measurements from sensor 1. The angle θ_{min} shows the angle closest to $\theta \to 0°$ (which is the 'exact' ram direction) and $I_+ (\theta_{min})$ shows the ion current as measured by sensor 1 for this specific angle. To obtain the correct $I_+ (\theta_{min})$ the plots mentioned earlier (i.e. $I_+ = f$ (G.M.T.)) and the detailed output from the tapes (in table form) were used. The same goes for θ_{max} and $I_+ (\theta_{max})$ except that for the maximum wake position $\theta \to 180°$. The column on the right shows the corresponding altitude. The column which gives Time (G.M.T.) is for our purposes of comparing information from plots with information from tables, and is of no value to the reader.

Table 2 also for sensor 1 provides the computed values of the nondimensional parameters:

$$R_D = \frac{R_o}{\lambda_D} = RD$$

$$\phi_N = \frac{e\phi_s}{KT_e} = PN$$

as well as the measured values of the plasma properties:

N_e = Density (=electron density)

T_e = Temp. (=electron temperature)

PS = ϕ_s (≡plasma potential)

VS = V_s (≡satellite velocity)

together with the corresponding values of α and H_o (≡altitude).

Table 1: Ion currents and angles of attack/Sensor 1

S3-2
ORBIT: 1131
DATE: 02/24/76

θ_{min}	$I_+(\theta_{min})$	θ_{max}	$I_+(\theta_{max})$	$\alpha=\frac{I_+(\theta_{max})}{I_+(\theta_{min})}$	Time$_o$(GMT)	H_o(Km)
43.56±1	4.40×10^{-9}	141.72±1	4.00×10^{-10}	9.1×10^{-2}	34624	1091.06
43.60±1	4.90×10^{-9}	141.75±1	4.20×10^{-10}	8.0×10^{-2}	34643	1079.03
43.63±1	5.81×10^{-9}	141.78±1	3.97×10^{-10}	6.8×10^{-2}	34662	1066.99
43.67±1	6.35×10^{-9}	141.82±1	4.45×10^{-10}	7.0×10^{-2}	34681	1054.98
43.70±1	6.90×10^{-9}	141.86±1	4.04×10^{-10}	5.9×10^{-2}	34700	1043.10
43.73±1	7.67×10^{-9}	141.88±1	4.03×10^{-10}	5.3×10^{-2}	34719	1031.07
43.77±1	7.62×10^{-9}	141.92±1	3.67×10^{-10}	4.8×10^{-2}	34738	1018.88
43.79±1	8.46×10^{-9}	141.95±1	3.44×10^{-10}	4.1×10^{-2}	34757	1006.38
43.82±1	8.14×10^{-9}	141.97±1	3.00×10^{-10}	3.7×10^{-2}	34776	993.85
43.85±1	8.22×10^{-9}	142.0 ±1	2.63×10^{-10}	3.2×10^{-2}	34795	981.28
43.87±1	7.85×10^{-9}	142.03±1	2.50×10^{-10}	3.2×10^{-2}	34814	968.69
43.90±1	8.89×10^{-9}	142.05±1	2.77×10^{-10}	3.1×10^{-2}	34833	956.06
43.92±1	9.50×10^{-9}	142.07±1	2.54×10^{-10}	2.7×10^{-2}	34852	943.41
43.95±1	9.91×10^{-9}	142.09±1	2.24×10^{-10}	2.3×10^{-2}	34871	930.72
43.97±1	9.40×10^{-9}	142.11±1	2.24×10^{-10}	2.4×10^{-2}	34890	918.01
43.99±1	9.08×10^{-9}	142.13±1	2.51×10^{-10}	2.8×10^{-2}	34909	905.26
44.01±1	9.91×10^{-9}	142.16±1	2.31×10^{-10}	2.3×10^{-2}	34928	892.46
44.03±1	8.26×10^{-9}	142.17±1	2.33×10^{-10}	2.8×10^{-2}	34947	879.64
44.04±1	9.06×10^{-9}	142.19±1	2.35×10^{-10}	2.6×10^{-2}	34966	866.81
44.06±1	8.60×10^{-9}	142.20±1	2.10×10^{-10}	2.4×10^{-2}	34985	853.99

Table 1: (cont'd) Sensor 1 (cont'd)

θ_{min}	$I_+(\theta_{min})$	θ_{max}	$I_+(\theta_{max})$	$\alpha=\frac{I_+(\theta_{max})}{I_+(\theta_{min})}$	T_o(GMT)	H_o(Km)
44.07±1	9.56×10^{-9}	142.21±1	2.12×10^{-10}	2.2×10^{-2}	35004	841.16
44.08±1	9.52×10^{-9}	142.22±1	1.99×10^{-10}	2.1×10^{-2}	35023	828.34
44.09±1	8.19×10^{-9}	142.23±1	1.96×10^{-10}	2.4×10^{-2}	35042	815.51
44.10±1	8.69×10^{-9}	142.24±1	2.08×10^{-10}	2.4×10^{-2}	35061	802.65
44.11±1	8.87×10^{-9}	142.25±1	1.60×10^{-10}	1.8×10^{-2}	35080	789.83
44.12±1	7.55×10^{-9}	142.26±1	1.91×10^{-10}	2.5×10^{-2}	35099	777.04
44.12±1	8.35×10^{-9}	142.26±1	1.68×10^{-10}	2.0×10^{-2}	35118	764.26
44.13±1	8.77×10^{-9}	142.27±1	1.70×10^{-10}	1.9×10^{-2}	35137	751.53
44.13±1	9.04×10^{-9}	142.27±1	1.75×10^{-10}	1.9×10^{-2}	35156	738.83
44.13±1	9.97×10^{-9}	142.27±1	1.8×10^{-10}	1.8×10^{-2}	35175	726.16
44.13±1	1.15×10^{-8}	142.27±1	1.98×10^{-10}	1.7×10^{-2}	35194	713.54
44.13±1	1.33×10^{-8}	142.27±1	2.24×10^{-10}	1.69×10^{-2}	35213	700.98
44.13±1	1.63×10^{-8}	142.26±1	2.41×10^{-10}	1.48×10^{-2}	35232	688.46
44.13±1	1.804×10^{-8}	142.26±1	2.406×10^{-10}	1.33×10^{-2}	35251	676.01
44.12±1	1.869×10^{-8}	142.25±1	2.161×10^{-10}	1.16×10^{-2}	35270	663.65
44.12±1	1.694×10^{-8}	142.25±1	1.972×10^{-10}	1.16×10^{-2}	35289	651.38
44.11±1	1.606×10^{-8}	142.24±1	1.734×10^{-10}	1.08×10^{-2}	35308	639.21
44.10±1	1.614×10^{-8}	142.23±1	1.584×10^{-10}	9.82×10^{-3}	35327	627.12
44.09±1	1.462×10^{-8}	142.22±1	1.405×10^{-10}	9.61×10^{-3}	35346	615.08
44.08±1	1.452×10^{-8}	142.21±1	1.278×10^{-10}	8.80×10^{-3}	35365	603.11

Table 1: (cont'd)

θ_{min}	$I_+(\theta_{min})$	θ_{max}	$I_+(\theta_{max})$	$\alpha=\frac{I_+(\theta_{max})}{I_+(\theta_{min})}$	T_o(GMT)	H_o(Km)
44.07±1	1.565×10^{-8}	142.19±1	1.240×10^{-10}	7.92×10^{-3}	35384	591.27
44.06±1	1.383×10^{-8}	142.18±1	1.180×10^{-10}	8.53×10^{-3}	35403	579.56
44.04±1	1.45×10^{-8}	142.17±1	1.245×10^{-10}	8.3×10^{-3}	35422	567.99
44.02±1	1.480×10^{-8}	142.15±1	1.231×10^{-10}	8.32×10^{-3}	35441	556.54
44.01±1	1.460×10^{-8}	142.13±1	1.298×10^{-10}	8.89×10^{-3}	35460	545.21
43.99±1	1.408×10^{-8}	142.12±1	1.289×10^{-10}	9.0×10^{-3}	35479	533.96
43.97±1	1.518×10^{-8}	142.09±1	1.333×10^{-10}	8.78×10^{-3}	35498	522.87
43.95±1	1.457×10^{-8}	142.07±1	1.241×10^{-10}	8.52×10^{-3}	35517	511.94
43.92±1	1.471×10^{-8}	142.05±1	1.2×10^{-10}	8.1×10^{-3}	35536	501.17
43.90±1	1.49×10^{-8}	142.03±1	1.121×10^{-10}	7.49×10^{-3}	35555	490.56
43.88±1	1.538×10^{-8}	142.00±1	1.057×10^{-10}	6.87×10^{-3}	35574	480.11
43.85±1	1.617×10^{-8}	141.98±1	9.5×10^{-11}	5.86×10^{-3}	35593	469.79
43.82±1	1.684×10^{-8}	141.95±1	8×10^{-11}	4.76×10^{-3}	35612	459.66
43.80±1	1.605×10^{-8}	141.92±1	0.524×10^{-10}	3.26×10^{-3}	35631	449.71
43.77±1	1.547×10^{-8}	141.89±1	0.423×10^{-10}	2.73×10^{-3}	35650	439.95
43.74±1	1.510×10^{-8}	141.86±1	3×10^{-11}	2.0×10^{-3}	35669	430.38
43.71±1	1.476×10^{-8}	141.82±1	3×10^{-11}	2.0×10^{-3}	35688	421.00
43.68±1	1.616×10^{-8}	141.79±1	0.275×10^{-10}	1.71×10^{-3}	35707	411.80
43.64±1	1.622×10^{-8}	141.76±1	0.150×10^{-10}	9.3×10^{-4}	35726	402.79
43.61±1	1.669×10^{-8}	141.73±1	1.2×10^{-11}	2.2×10^{-4}	35745	393.99

Table 1: (cont'd)

θ_{min}	$I_+(\theta_{min})$	θ_{max}	$I_+(\theta_{max})$	$\alpha=\frac{I_+(\theta_{max})}{I_+(\theta_{min})}$	T_o(GMT)	H_o(Km)
43.57±1	1.786×10^{-8}	141.69±1	7.5×10^{-12}	4.2×10^{-4}	35764	385.42
43.54±1	2.142×10^{-8}	141.66±1	7.1×10^{-12}	3.3×10^{-4}	35783	377.06
43.50±1	2.451×10^{-8}	141.62±1	6.0×10^{-12}	2.45×10^{-4}	35802	368.93
43.46±1	2.451×10^{-8}	141.58±1	0.3×10^{-11}	1.22×10^{-4}	35821	361.02
43.42±1	2.594×10^{-8}	141.54±1	0.3×10^{-11}	1.15×10^{-4}	35840	353.31
43.34±1	3.108×10^{-8}	141.45±1	0.392×10^{-11}	1.26×10^{-4}	35878	338.60
43.29±1	3.322×10^{-8}	141.41±1	2.8×10^{-12}	8.4×10^{-5}	35897	331.56
43.35±1	3.776×10^{-8}	141.36±1	0.181×10^{-11}	4.76×10^{-5}	35916	324.78
43.11±1	5.031×10^{-8}	141.22±1	0.267×10^{-11}	5.29×10^{-5}	35973	306.00
43.06±1	5.054×10^{-8}	141.17±1	0.9×10^{-12}	1.81×10^{-5}	35992	300.25

TABLE 2: Plasma Parameters — Sensor 1

Density	PS	Temp.	VS	RD	PN	α	Ho(km)
0.377×10^4	-1.17	1006.	7.299	27.86	-13.52	3.7×10^{-2}	993.85
0.367×10^4	-1.17	1006.	7.311	26.25	-13.52	3.2×10^{-2}	981.28
0.342×10^4	-1.34	1180.	7.324	24.67	-13.20	3.2×10^{-2}	968.69
0.368×10^4	-1.22	1011.	7.337	28.33	-14.11	3.1×10^{-2}	956.06
0.405×10^4	-1.19	963.	7.349	29.46	-14.37	2.7×10^{-2}	943.41
0.411×10^4	-1.19	963.	7.362	29.35	-14.37	2.3×10^{-2}	930.72
0.414×10^4	-1.19	963.	7.375	30.05	-14.37	2.4×10^{-2}	918.01
0.437×10^4	-1.09	976.	7.387	30.63	-12.99	2.8×10^{-2}	905.26
0.427×10^4	-1.04	1053.	7.400	28.39	-11.50	2.3×10^{-2}	892.46
0.437×10^4	-1.01	1092.	7.413	28.72	-10.75	2.8×10^{-2}	879.64
0.450×10^4	-1.09	1026.	7.426	30.85	-12.35	2.6×10^{-2}	866.81
0.480×10^4	-1.09	1026.	7.439	31.35	-12.35	2.4×10^{-2}	853.99
0.481×10^4	-1.09	1026.	7.452	31.54	-12.35	2.2×10^{-2}	841.16
0.456×10^4	-1.08	1032.	7.465	30.17	-12.16	2.1×10^{-2}	828.34
0.423×10^4	-1.07	1036.	7.478	29.28	-12.01	2.4×10^{-2}	815.51
0.410×10^4	-1.08	954.	7.491	30.04	-13.16	2.4×10^{-2}	802.65
0.391×10^4	-1.08	954.	7.504	29.34	-13.16	1.8×10^{-2}	789.83
0.392×10^4	-1.13	963.	7.517	28.83	-13.64	2.5×10^{-2}	777.04
0.393×10^4	-1.13	963.	7.531	29.54	-13.64	2.0×10^{-2}	764.26
0.406×10^4	-1.13	963.	7.544	29.61	-13.64	1.9×10^{-2}	751.53
0.432×10^4	-1.08	1207.	7.557	27.42	-10.40	1.9×10^{-2}	738.83
0.472×10^4	-1.08	1207.	7.570	28.66	-10.40	1.8×10^{-2}	726.16
0.551×10^4	-1.19	1123.	7.583	32.10	-12.32	1.7×10^{-2}	713.54
0.689×10^4	-1.21	1185.	7.596	34.94	-11.89	1.69×10^{-2}	700.98
0.822×10^4	-1.24	1308.	7.609	36.50	-11.02	1.48×10^{-2}	688.46

TABLE 2: Plasma Parameters (cont) Sensor 1

Density	PS	Temp.	VS	RD	PN	α	Ho(km)
0.968×10^4	-1.24	1308.	7.622	39.41	-11.02	1.33×10^{-2}	676.01
0.981×10^4	-1.24	1308.	7.635	39.68	-11.02	1.16×10^{-2}	663.65
0.960×10^4	-1.32	1254.	7.648	40.04	-12.24	1.16×10^{-2}	651.38
0.955×10^4	-1.35	1302.	7.660	39.38	-12.11	1.08×10^{-2}	639.21
0.954×10^4	-1.47	1468.	7.673	36.94	-11.64	9.82×10^{-3}	627.12
0.981×10^4	-1.20	1116.	7.686	43.83	-12.57	9.61×10^{-3}	615.08
0.949×10^4	-1.17	1072.	7.699	43.30	-12.69	8.80×10^{-3}	603.11
0.959×10^4	-1.17	1072.	7.712	43.9	-12.69	7.92×10^{-3}	591.27
0.916×10^4	-1.21	1114.	7.724	42.36	-12.66	8.53×10^{-3}	579.56
0.930×10^4	-1.55	1449.	7.736	36.69	-12.44	8.3×10^{-3}	567.99
0.967×10^4	-1.37	1415.	7.748	38.02	-11.26	8.32×10^{-3}	556.54
0.942×10^4	-1.32	1405.	7.761	37.51	-10.92	8.89×10^{-3}	545.21
0.953×10^4	-1.48	1278.	7.773	39.55	-13.47	9.0×10^{-3}	533.96
0.960×10^4	-1.48	1278.	7.785	39.70	-13.47	8.78×10^{-3}	522.87
0.992×10^4	-1.48	1278.	7.797	40.34	-13.47	8.52×10^{-3}	511.94
1.01×10^4	-1.44	1367.	7.808	39.82	-12.28	8.10×10^{-3}	501.17
1.05×10^4	-1.42	1412.	7.820	39.46	-11.69	7.49×10^{-3}	490.56
1.10×10^4	-1.56	1260.	7.831	42.70	-14.40	6.87×10^{-3}	480.11
1.20×10^4	-1.56	1260.	7.842	44.67	-14.40	5.86×10^{-3}	469.79
1.18×10^4	-1.87	1637.	7.853	38.98	-13.28	4.76×10^{-3}	459.66
1.13×10^4	-1.87	1637.	7.864	38.14	-13.28	3.26×10^{-3}	449.71
1.13×10^4	-1.87	1637.	7.875	38.07	-13.28	2.73×10^{-3}	439.95
1.05×10^4	-1.70	1223.	7.885	42.51	-16.16	2.0×10^{-3}	430.38
1.12×10^4	-1.70	1223.	7.896	43.87	-16.16	2.0×10^{-3}	421.00
1.14×10^4	-1.99	1535.	7.906	39.43	-15.07	1.71×10^{-3}	411.80

TABLE 2: Plasma Parameters (cont) Sensor 1

Density	PS	Temp.	VS	RD	PN	α	Ho(km)
1.16×10^4	-1.99	1434.	7.916	41.52	-16.27	9.3×10^{-4}	402.79
1.17×10^4	-2.00	1308.	7.926	43.38	-17.78	7.2×10^{-4}	393.79
1.27×10^4	-2.00	1308.	7.936	45.11	-17.78	4.2×10^{-4}	385.42
1.40×10^4	-2.00	1308.	7.945	47.43	-17.78	3.3×10^{-4}	377.06
1.51×10^4	-1.95	1564.	7.954	44.98	-14.50	2.45×10^{-4}	368.93
1.56×10^4	-2.10	1732.	7.963	43.75	-14.16	1.22×10^{-4}	361.02
1.56×10^4	-2.40	2069.	7.972	39.78	-13.49	1.15×10^{-4}	353.31
1.50×10^4	-1.92	1609.	7.981	44.18	-13.88		345.84
1.73×10^4	-1.92	1609.	7.989	47.52	-13.88	1.26×10^{-4}	338.60
1.86×10^4	-1.92	1609.	7.997	49.21	-13.88	8.4×10^{-5}	331.56
2.04×10^4	-1.98	1791.	8.004	50.11	-13.12	4.76×10^{-5}	324.78
2.17×10^4	-2.19	2430.	8.012	43.34	-10.48		318.25
2.13×10^4	-1.87	1690.	8.019	52.84	-13.08		312.00
2.27×10^4	-1.84	1597.	8.026	54.63	-13.40	5.29×10^{-5}	306.00
2.24×10^4	-1.91	1566.	8.033	54.87	-14.18	1.8×10^{-5}	300.25
2.23×10^4	-1.91	1566.	8.039	54.69	-14.18		294.74
2.25×10^4	-1.91	1566.	8.045	54.87	-14.18		289.48
1.89×10^4	-1.86	1678.	8.051	48.52	-12.93		284.50
1.95×10^4	-1.85	1710.	8.056	48.91	-12.58	4.0×10^{-5}	279.78
1.90×10^4	-1.93	1476.	8.062	51.90	-15.20		275.34
1.84×10^4	-1.93	1476.	8.067	51.20	-15.20		271.17

Table 3: Ion currents and angles of attack/Sensor 5

S3-2
ORBIT: 1131
DATE: 02/24/76

θ_{min}	$I_+(\theta_{min})$	θ_{max}	$I_+(\theta_{max})$	$\alpha=\frac{I_+(\theta_{max})}{I_+(\theta_{min})}$	Time$_o$ (GMT)	H_o (Km)
42.34±1	2.537×10^{-9}	142.98±1	2.015×10^{-10}	7.94×10^{-2}		1085
42.38±1	2.998×10^{-9}	143.01±1	2.319×10^{-10}	7.74×10^{-2}		1073
42.41±1	3.388×10^{-9}	143.05±1	2.435×10^{-10}	7.19×10^{-2}		
42.44±1	3.812×10^{-9}	143.08±1	2.410×10^{-10}	6.32×10^{-2}	34700	1043.10
42.48±1	4.061×10^{-9}	143.11±1	2.421×10^{-10}	5.96×10^{-2}		1037
42.51±1	4.296×10^{-9}	143.15±1	1.955×10^{-10}	4.55×10^{-2}		
42.54±1	4.288×10^{-9}	143.17±1	2.057×10^{-10}	4.80×10^{-2}	34747	1012.97
42.57±1	4.248×10^{-9}	143.20±1	1.560×10^{-10}	3.67×10^{-2}	34776	993.85
42.59±1	3.993×10^{-9}	143.23±1	1.422×10^{-10}	3.56×10^{-2}	34786	987.24
42.62±1	3.521×10^{-9}	143.25±1	1.111×10^{-10}	3.16×10^{-2}	34805	974.66
42.65±1	3.595×10^{-9}	143.28±1	1.241×10^{-10}	3.45×10^{-2}	34824	962.05
42.67±1	4.040×10^{-9}	143.30±1	1.044×10^{-10}	2.1×10^{-2}	34843	949.41
42.71±1	4.001×10^{-9}	143.35±1	8.0×10^{-11}	2.0×10^{-2}	34881	924.03
42.73±1	4.217×10^{-9}	143.37±1	9.756×10^{-11}	2.4×10^{-2}	34900	911.30
42.75±1	4.180×10^{-9}	143.39±1	1.01×10^{-10}	2.4×10^{-2}	34919	898.54
42.78±1	3.778×10^{-9}	143.40±1	8×10^{-11}	2.3×10^{-2}	34938	885.71
42.80±1	4.020×10^{-9}	143.42±1	1.017×10^{-10}	2.53×10^{-2}	34957	872.89
42.81±1	4.063×10^{-9}	143.44±1	9.431×10^{-11}	2.32×10^{-2}	34976	860.06
42.82±1	4.354×10^{-9}	143.45±1	8.698×10^{-11}	2.00×10^{-2}	34995	847.24

Table 3: (cont'd) Sensor 5 (cont'd)

θ_{min}	$I_+(\theta_{min})$	θ_{max}	$I_+(\theta_{max})$	$\alpha=\frac{I_+(\theta_{max})}{I_+(\theta_{min})}$	T_o (GMT)	H_o (Km)
42.83±1	4.585×10^{-9}	143.46±1	8.920×10^{-11}	1.95×10^{-2}	35014	834.41
42.84±1	4.086×10^{-9}	143.47±1	1.010×10^{-10}	2.47×10^{-2}	35033	821.59
42.85±1	4.080×10^{-9}	143.48±1	1.017×10^{-10}	2.49×10^{-2}	35052	808.74
42.86±1	4.192×10^{-9}	143.49±1	1.030×10^{-10}	2.46×10^{-2}	35071	795.90
42.87±1	3.808×10^{-9}	143.50±1	9.0×10^{-11}	2.37×10^{-2}	35090	783.09
42.88±1	4.211×10^{-9}	143.50±1	9.720×10^{-11}	2.31×10^{-2}	35109	770.31
42.88±1	4.257×10^{-9}	143.51±1	8.942×10^{-11}	2.10×10^{-2}	35128	757.56
42.89±1	4.392×10^{-9}	143.51±1	8.410×10^{-11}	1.91×10^{-2}	35147	744.84
42.89±1	4.591×10^{-9}	143.51±1	8.777×10^{-11}	1.92×10^{-2}	35166	732.16
42.89±1	5.5×10^{-9}	143.51±1	9.0×10^{-11}	1.64×10^{-2}	35185	719.51
42.89±1	5.727×10^{-9}	143.51±1	9.209×10^{-11}	1.67×10^{-2}	35204	706.92
42.89±1	6.729×10^{-9}	143.51±1	9.985×10^{-11}	1.48×10^{-2}	35223	694.39
42.88±1	7.769×10^{-9}	143.50±1	9.255×10^{-11}	1.19×10^{-2}	35242	681.89
42.88±1	8.164×10^{-9}	143.50±1	8.218×10^{-11}	1.01×10^{-2}	35261	669.49
42.88±1	8.0×10^{-9}	143.49±1	9×10^{-11}	1.14×10^{-2}	35280	657.18
42.87±1	7.434×10^{-9}	143.49±1	7.5×10^{-11}	1.0×10^{-2}	35299	644.97
42.86±1	7.307×10^{-9}	143.48±1	7.3×10^{-11}	1.0×10^{-2}	35318	632.83
42.85±1	7.391×10^{-9}	143.47±1	7.0×10^{-11}	9.5×10^{-3}	35337	620.78
42.84±1	7.214×10^{-9}	143.46±1	6.0×10^{-11}	8.3×10^{-3}	35356	608.76
42.83±1	7.139×10^{-9}	143.45±1	5.193×10^{-11}	7.27×10^{-3}	35375	596.86

Table 3: (cont'd)

θ_{min}	$I_+(\theta_{min})$	θ_{max}	$I_+(\theta_{max})$	$\alpha=\frac{I_+(\theta_{max})}{I_+(\theta_{min})}$	T_o(GMT)	H_o(Km)
42.82±1	7.197×10^{-9}	143.43±1	5.0×10^{-11}	6.9×10^{-3}	35394	585.09
42.80±1	6.850×10^{-9}	143.42±1	5.0×10^{-11}	7.3×10^{-3}	35413	573.46
42.79±1	6.885×10^{-9}	143.40±1	4.9×10^{-11}	7.1×10^{-3}	35432	561.95
42.77±1	6.843×10^{-9}	143.39±1	4.5×10^{-11}	6.6×10^{-3}	35451	550.56
42.76±1	6.862×10^{-9}	143.37±1	4.0×10^{-11}	5.8×10^{-3}	35470	539.27
42.74±1	6.907×10^{-9}	143.35±1	3.8×10^{-11}	5.5×10^{-3}	35489	528.10
42.70±1	7.210×10^{-9}	143.30±1	4.0×10^{-11}	5.6×10^{-3}	35527	506.25
42.67±1	7.418×10^{-9}	143.28±1	3.4×10^{-11}	4.6×10^{-3}	35546	495.56
42.65±1	8.062×10^{-9}	143.25±1	3.1×10^{-11}	3.8×10^{-3}	35565	485.04
42.63±1	8.789×10^{-9}	143.23±1	3.25×10^{-11}	3.7×10^{-3}	35584	474.66
42.60±1	9.331×10^{-9}	143.20±1	2.8×10^{-11}	3.0×10^{-3}	35603	464.43
42.57±1	1.035×10^{-8}	143.18±1	2.7×10^{-11}	2.6×10^{-3}	35622	454.40
42.54±1	1.075×10^{-8}	143.15±1	2.6×10^{-11}	2.36×10^{-3}	35641	444.55
42.51±1	1.123×10^{-8}	143.12±1	2.0×10^{-11}	1.8×10^{-3}	35660	434.89
42.48±1	1.168×10^{-8}	143.09±1	1.5×10^{-11}	1.3×10^{-3}	35679	425.42
42.45±1	1.212×10^{-8}	143.05±1	8.5×10^{-12}	7.04×10^{-4}	35698	416.15
42.42±1	1.372×10^{-8}	143.02±1	8×10^{-12}	5.7×10^{-4}	35717	407.03
42.38±1	1.439×10^{-8}	142.99±1	7.8×10^{-12}	5.4×10^{-4}	35736	398.13
42.03±1	3.207×10^{-8}	142.63±1	1.853×10^{-11}	5.78×10^{-4}	35907	327.96
41.99±1	3.846×10^{-8}	142.58±1	1.853×10^{-11}	4.82×10^{-4}	35926	321.31

Table 3: (cont'd)

θ_{min}	$I_+(\theta_{min})$	θ_{max}	$I_+(\theta_{max})$	$\alpha=\frac{I_+(\theta_{max})}{I_+(\theta_{min})}$	T_o (GMT)	H_o (Km)
41.94±1	3.982×10^{-8}	142.54±1	1.872×10^{-10}	4.70×10^{-3}	35945	314.93
41.89±1	4.335×10^{-8}	142.49±1	1.872×10^{-10}	4.32×10^{-3}	35964	308.81
41.70±1	4.086×10^{-8}	142.29±1	4.437×10^{-11}	1.09×10^{-3}	36040	286.83

TABLE 4: Plasma Parameters

Sensor 5

Density	PS	Temp.	VS	RD	PN	$\alpha=\frac{I+(\theta max)}{I+(\theta min)}$	Ho(km)
$4.11x10^{3}$	-1.17	1006.	7.306	29.27	-13.52	$3.56x10^{-2}$	987.24
$3.86x10^{3}$	-1.34	1180.	7.318	26.20	-13.20	$3.16x10^{-2}$	974.66
$3.99x10^{3}$	-1.34	1180.	7.331	26.63	-13.20	$3.45x10^{-2}$	962.05
$4.46x10^{3}$	-1.19	963.	7.343	31.17	-14.37	$2.1x10^{-2}$	949.41
$4.70x10^{3}$	-1.19	963.	7.356	32.01	-14.37		936.73
$4.55x10^{3}$	-1.19	963.	7.369	31.49	-14.37	$2.0x10^{-2}$	924.03
$4.98x10^{3}$	-1.09	976.	7.381	32.74	-12.99	$2.4x10^{-2}$	911.30
$4.99x10^{3}$	-1.09	976.	7.394	32.78	-12.99	$2.4x10^{-2}$	898.54
$4.56x10^{3}$	-1.01	1092.	7.407	29.61	-10.75	$2.3x10^{-2}$	885.71
$4.75x10^{3}$	-1.04	1070.	7.420	30.47	-11.28	$2.53x10^{-2}$	872.89
$5.03x10^{3}$	-1.09	1026.	7.433	32.09	-12.35	$2.32x10^{-2}$	860.06
$5.37x10^{3}$	-1.09	1026.	7.446	33.16	-12.35	$2.00x10^{-2}$	847.24
$5.46x10^{3}$	-1.09	1026.	7.459	33.42	-12.35	$1.95x10^{-2}$	834.41
$4.88x10^{3}$	-1.07	1036.	7.472	31.45	-12.01	$2.47x10^{-2}$	821.59
$4.54x10^{3}$	-1.07	1018.	7.485	30.55	-12.27	$2.49x10^{-2}$	808.74
$4.46x10^{3}$	-1.08	954.	7.498	31.35	-13.16	$2.46x10^{-2}$	795.90
$4.44x10^{3}$	-1.12	962.	7.511	31.13	-13.59	$2.37x10^{-2}$	783.09
$4.27x10^{3}$	-1.13	963.	7.524	30.53	-13.64	$2.31x10^{-2}$	770.31
$4.37x10^{3}$	-1.13	963.	7.538	30.86	-13.64	$2.10x10^{-2}$	757.56
$4.57x10^{3}$	-1.12	990.	7.551	31.55	-13.28	$1.91x10^{-2}$	744.84
$4.95x10^{3}$	-1.08	1207.	7.564	29.34	-10.40	$1.92x10^{-2}$	732.16
$5.87x10^{3}$	-1.16	1141.	7.577	33.13	-11.89	$1.64x10^{-2}$	719.51
$6.72x10^{3}$	-1.19	1123.	7.590	35.44	-12.32	$1.67x10^{-2}$	706.92
$8.25x10^{3}$	-1.24	1308.	7.603	36.38	-11.02	$1.48x10^{-2}$	794.39
$9.49x10^{3}$	-1.24	1308.	7.616	39.72	-11.02	$1.19x10^{-2}$	681.89

TABLE 4: Plasma Parameters (cont) Sensor 5

Density	PS	Temp.	VS	RD	PN	$\alpha=\frac{I+(\theta max)}{I+(\theta min)}$	Ho(km)
$1.05x10^4$	-1.24	1308.	7.629	41.12	-11.02	$1.01x10^{-2}$	669.49
$1.14x10^4$	-1.29	1272.	7.642	42.07	-11.83	$1.1x10^{-2}$	657.18
$1.04x10^4$	-1.32	1254.	7.654	41.78	-12.24	$1.0x10^{-2}$	644.97
$1.28x10^4$	-1.47	1468.	7.667	38.34	-11.64	$1.0x10^{-2}$	632.83
$1.06x10^4$	-1.47	1468.	7.680	38.84	-11.64	$9.5x10^{-3}$	620.78
$1.02x10^4$	-1.17	1072.	7.693	44.76	-12.69	$8.3x10^{-3}$	608.76
$1.05x10^4$	-1.17	1072.	7.705	45.32	-12.69	$7.27x10^{-3}$	596.86
$9.98x10^3$	-1.17	1072.	7.718	44.22	-12.69	$6.9x10^{-3}$	585.09
$9.73x10^3$	-1.55	1449.	7.730	37.54	-12.44	$7.3x10^{-3}$	573.46
$9.64x10^3$	-1.55	1449.	7.743	37.36	-12.44	$7.1x10^{-3}$	561.95
$9.42x10^3$	-1.32	1405.	7.755	37.52	-10.92	$6.6x10^{-3}$	550.56
$9.41x10^3$	-1.39	1349.	7.767	38.38	-12.05	$5.8x10^{-3}$	539.27
$9.43x10^3$	-1.48	1278.	7.779	39.36	-13.47	$5.5x10^{-3}$	528.10
$9.57x10^3$	-1.48	1278.	7.791	39.65	-13.47		517.09
$9.78x10^3$	-1.48	1278.	7.803	40.08	-13.47	$5.6x10^{-3}$	506.25
$9.80x10^3$	-1.42	1412.	7.814	38.18	-11.69	$4.6x10^{-3}$	495.56
$1.05x10^4$	-1.47	1361.	7.826	40.24	-12.59	$3.8x10^{-3}$	485.04
$1.10x10^4$	-1.56	1260.	7.837	42.72	-14.40	$3.7x10^{-3}$	474.66
$1.12x10^4$	-1.87	1637.	7.848	37.96	-13.28	$3.0x10^{-3}$	464.43
$1.14x10^4$	-1.87	1637.	7.859	38.15	-13.28	$2.6x10^{-3}$	454.40
$1.1x10^4$	-1.87	1637.	7.870	37.51	-13.28	$2.36x10^{-3}$	444.55
$1.12x10^4$	-1.83	1545.	7.880	38.75	-13.92	$1.8x10^{-3}$	434.89
$1.06x10^4$	-1.70	1223.	7.891	42.64	-16.16	$1.3x10^{-3}$	425.42
$1.03x10^4$	-1.96	1500.	7.901	37.60	-15.19	$7.0x10^{-4}$	416.15
$1.13x10^4$	-1.99	1535.	7.912	39.28	-15.07	$5.7x10^{-4}$	407.03
$1.10x10^4$	-2.00	1308.	7.922	41.93	-17.78	$5.4x10^{-4}$	398.13

TABLE 4: Plasma Parameters (cont) Sensor 5

Density	PS	Temp.	VS	RD	PN	$\alpha=\frac{I+(\theta max)}{I+(\theta min)}$	Ho(km)
$1.21x10^4$	-2.00	1308.	7.932	43.97	-17.78		389.45
$1.31x10^4$	-2.00	1308.	7.941	45.82	-17.78		380.99
$1.39x10^4$	-1.96	1507.	7.950	43.76	-15.23		372.75
$1.51x10^4$	-1.95	1564.	7.959	45.01	-14.50		364.74
$1.44x10^4$	-2.40	2069.	7.968	38.18	-13.49		356.93
$1.63x10^4$	-2.40	2069.	7.977	40.61	-13.49		349.35
$1.58x10^4$	-1.92	1609.	7.985	45.41	-13.88		342.00
$1.64x10^4$	-1.92	1609.	7.993	46.23	-13.88		334.86
$1.87x10^4$	-1.92	1609.	8.001	49.41	-13.88	$5.78x10^{-4}$	327.96
$2.00x10^4$	-2.10	2430.	8.008	41.57	-10.48	$4.82x10^{-4}$	321.31
$2.18x10^4$	-2.19	2430.	8.016	43.43	-10.48	$4.70x10^{-3}$	314.93
$2.20x10^4$	-1.84	1597.	8.023	53.83	-13.40	$4.32x10^{-3}$	308.81
$2.17x10^4$	-1.89	1580.	8.030	53.71	-13.83		302.94
$2.22x10^4$	-1.91	1566.	8.036	54.57	-14.18		297.32
$2.22x10^4$	-1.91	1566.	8.042	54.54	-14.18		291.94
$2.10x10^4$	-1.91	1566.	8.048	53.07	-14.18	$1.09x10^{-3}$	286.83
$1.68x10^4$	-1.85	1710.	8.054	45.35	-12.58		281.98
$1.81x10^4$	-1.89	1606.	8.059	48.43	-13.74		277.41
$1.81x10^4$	-1.93	1476.	8.064	50.72	-15.20		273.11
$1.35x10^4$	-2.37	2770.	8.069	31.93	-9.95		269.08

Tables 3 and 4 present the similar information for sensor 5. We have chosen to provide in this report results for one sensor from each probe assembly (front & back) only. Calculations, however, were made for each of the sensors.

In summary: We have a relatively meaningful sample of:

$$\alpha = \frac{I_+ (\theta_{max})}{I_+ (\theta_{min})} \approx \frac{I_+ \text{ (wake)}}{I_+ \text{ (front)}}$$

$$\approx \frac{I_+ \text{ (wake)}}{I_+ \text{ (ambient)}}$$

which lends itself to a physical parametric analysis such as: $\alpha = f(R_D, \phi_N)$. Figure 1 shows the variation of $\alpha = \left[\frac{I_+ \text{ (wake)}}{I_+ \text{ (front)}}\right]$ with altitude using measurements from sensors 1,2,3 (i.e. from the forward probe assembly). It is seen that the variation in α extends over four orders of magnitude in the altitude range 300 km to 1100 km. The steepest variation being in the altitude range 300 km to 500 km. Figure 2 shows the variation of $R_D = f(H)$. It is seen that the largest variation in $R_D (= R_o/\lambda_D)$ is in the altitude range 300 km to (450-500) km. Figure 3 is obtained basically from Fig. 1 and Fig. 2 and shows the variation of $\alpha = f(R_D)$. The result obtained shows that the case of a 'large-body' becomes applicable for $R_D \approx 40$. This is a new experimental finding which is relevant to spacelab applications and is of importance to theoretical wake modeling. In other words: Figures 1 - 3 show that the amount of ion depletion in the wake of an ionospheric satellite for $R_D \geq 40$ is several orders of magnitude larger than for the cases were $24 < R_D < 40$. The behaviour of $R_D = f(H)$ in the altitude range 600 km to 700 km requires further study.

We have repeated the same procedure for the measurements made by sensors 5, 6, and 8. As seen from Figure 4 ($\alpha=f(H)$) the data is of lower quality compared with the data from sensors 1, 2, and 3 but still depicts qualitatively the general behaviour as seen in Figure 1.

We have also plotted $[M_+]_{AV}=f(H)$ (Figure 5) in order to study $\alpha = f(S_{AV})$ where: S_{AV} = average ionic Mach number. No clear correlation can at this point of the study be pointed out. We have also examined $\alpha = f(\phi_N)$. As seen from Figures 6 and 7 no obvious correlation between α and ϕ_N is obvious. In fact from Figure 6 we see that values of α which differ by about two orders of magnitude have similar values of ϕ_N (i.e., $12.5<|\phi_N|<15$) which can point to the fact that another parametric dependence is dominant. And indeed based on the present sample of measurements we believe that $\alpha = f(R_D)$ is dominant.

Note: The above results (as an experimental finding) is publishable. We believe it is adequate for the Journal of Geophysical Research Letters.

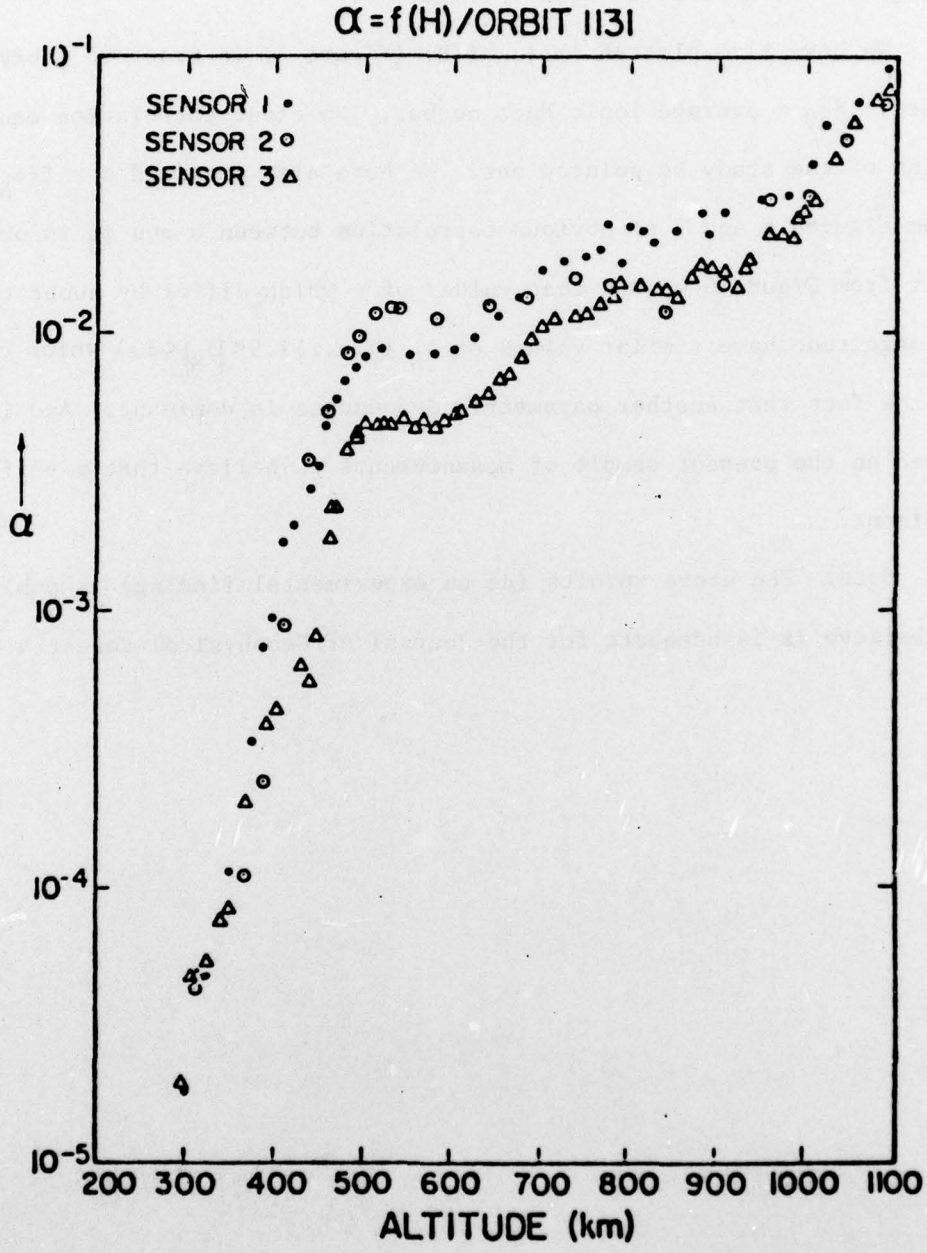
α = f(H)/ORBIT 1131
SENSOR 1 •
SENSOR 2 o
SENSOR 3 Δ
10^-1
10^-2
10^-3
10^-4
10^-5
α
200 300 400 500 600 700 800 900 1000 1100
ALTITUDE (km)

FIGURE 1

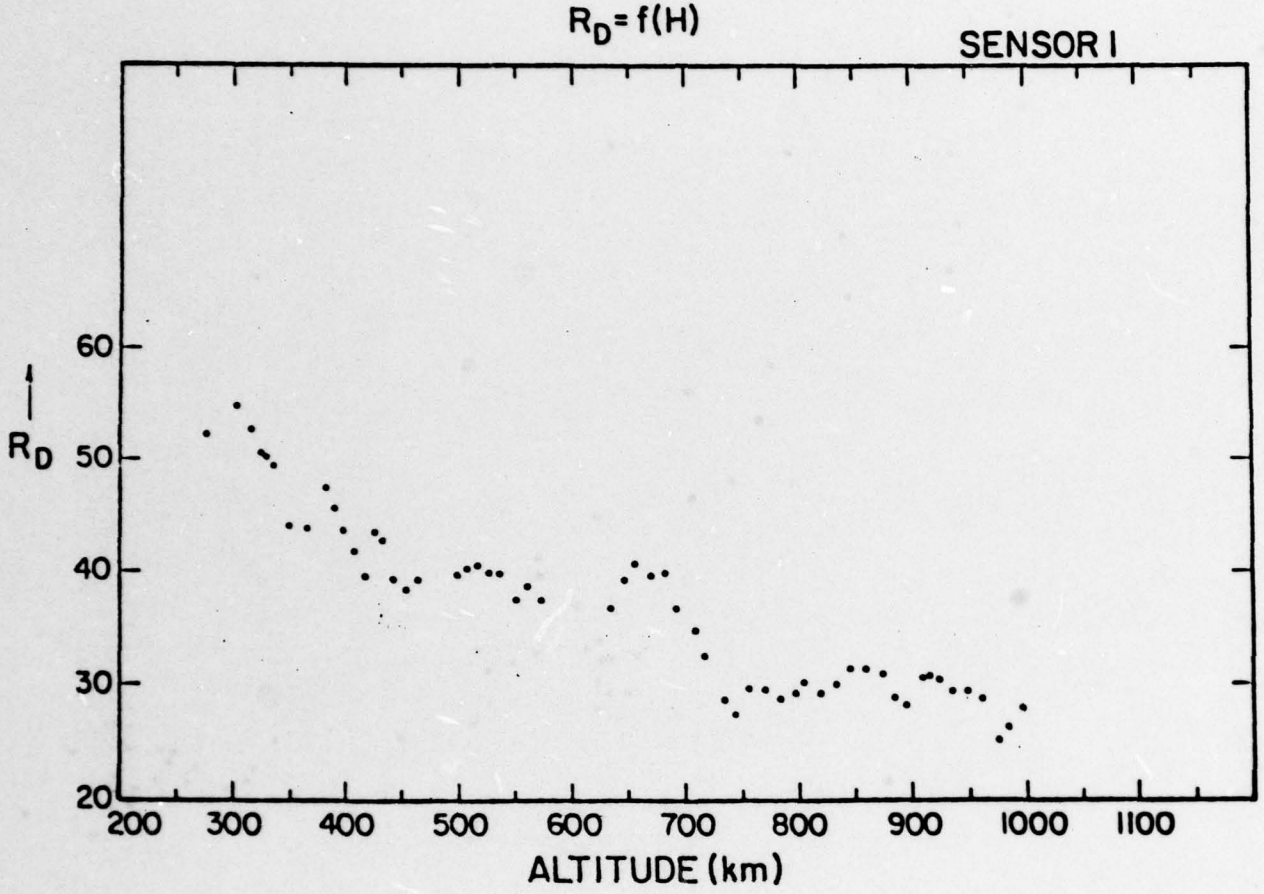
$R_D = f(H)$
SENSOR I
R_D
60
50
40
30
20
200
300
400
500
600
700
800
900
1000
1100
ALTITUDE (km)

FIGURE 2

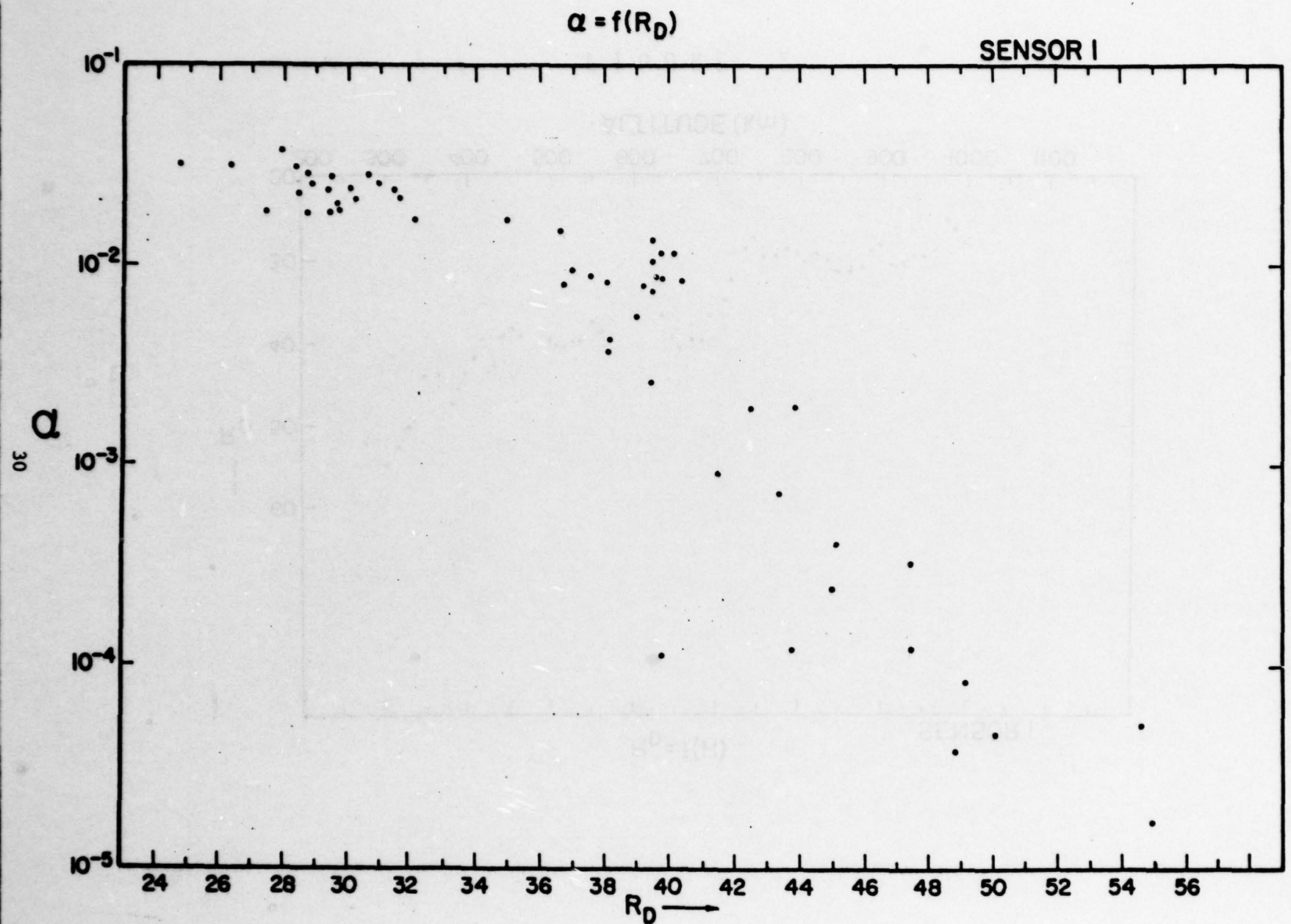
α = f(R_D)
SENSOR I
10^-1
10^-2
10^-3
10^-4
10^-5
α30
24
26
28
30
32
34
36
38
40
42
44
46
48
50
52
54
56
R_D

FIGURE 3

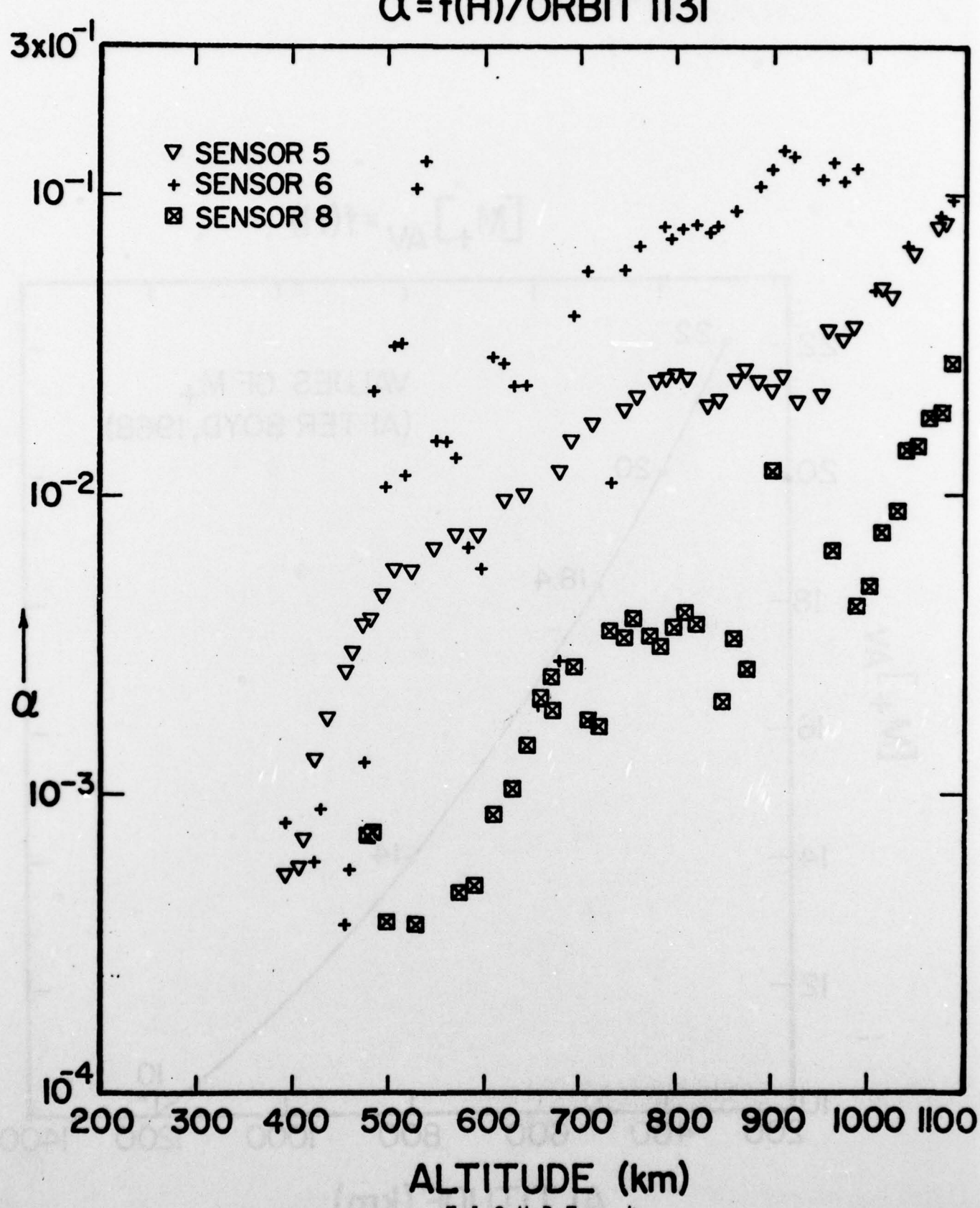
α = f(H)/ORBIT 1131
3x10⁻¹
10⁻¹
10⁻²
10⁻³
10⁻⁴
α
SENSOR 5
SENSOR 6
SENSOR 8
200
300
400
500
600
700
800
900
1000
1100
ALTITUDE (km)

FIGURE 4

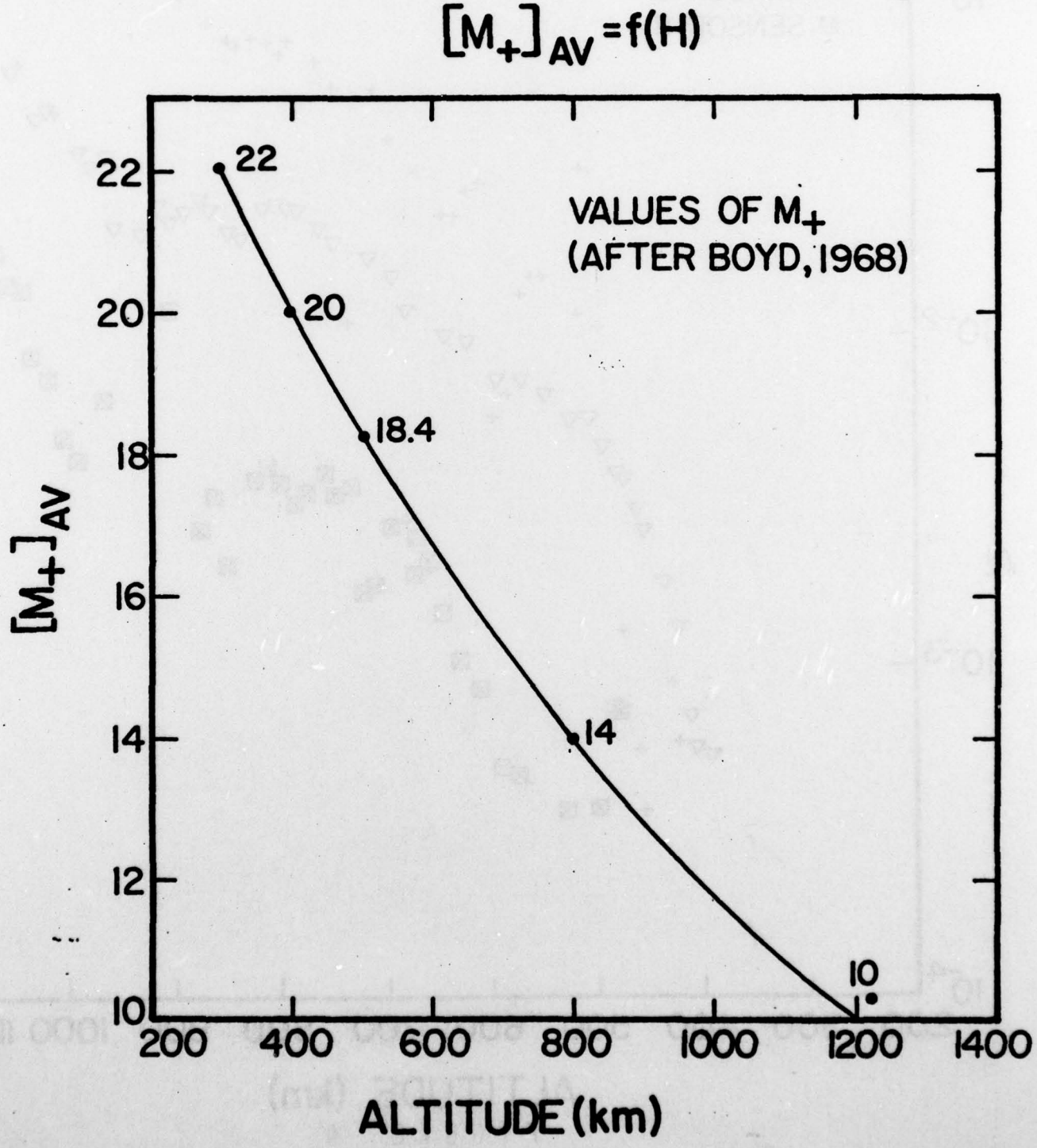
$[M_+]_{AV} = f(H)$
VALUES OF M_+
(AFTER BOYD, 1968)
22
20
18.4
14
10
$[M_+]_{AV}$
22
20
18
16
14
12
10
200
400
600
800
1000
1200
1400
ALTITUDE (km)

FIGURE 5

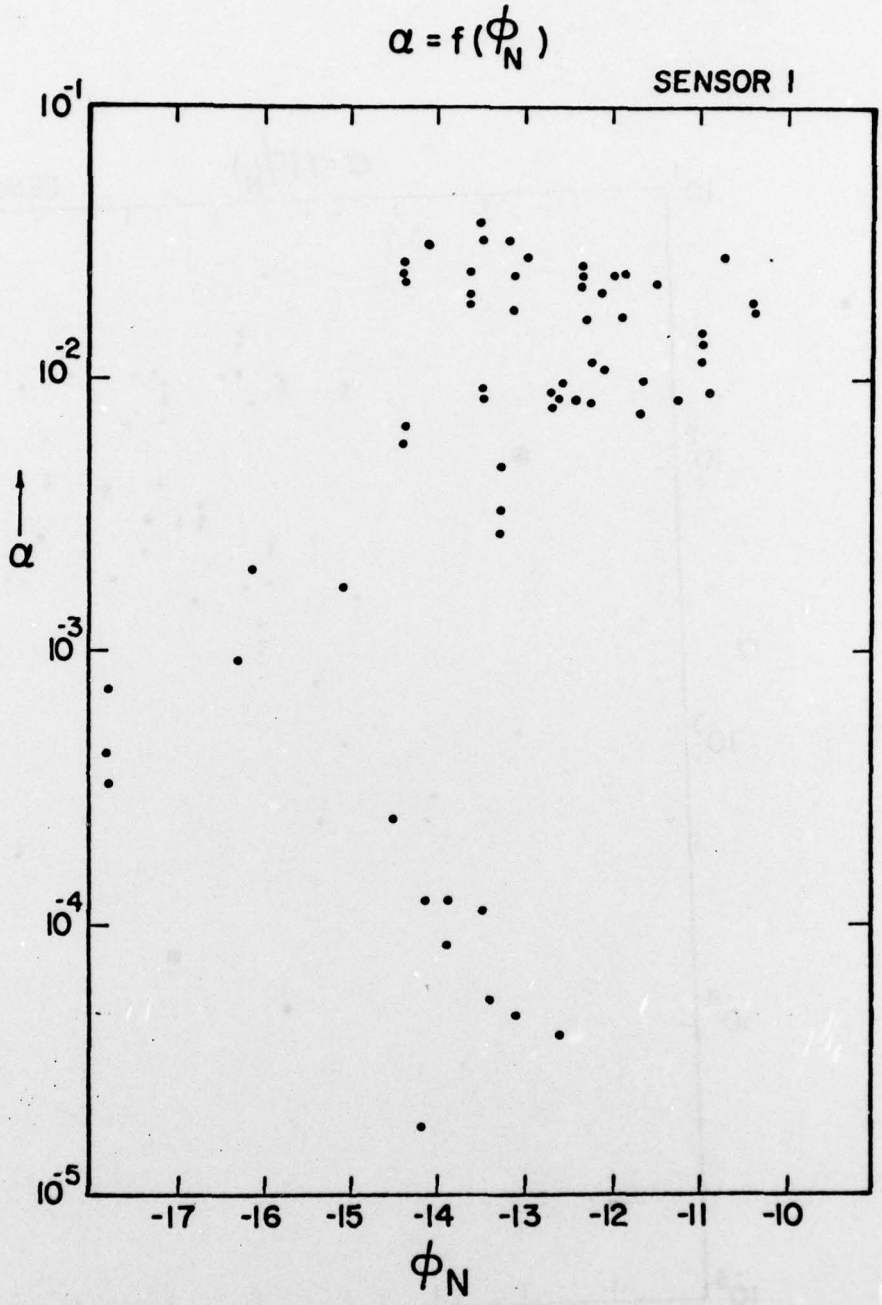
$\alpha = f(\phi_N)$
SENSOR 1
10^{-1}
10^{-2}
10^{-3}
10^{-4}
10^{-5}
α
-17
-16
-15
-14
-13
-12
-11
-10
ϕ_N

FIGURE 6

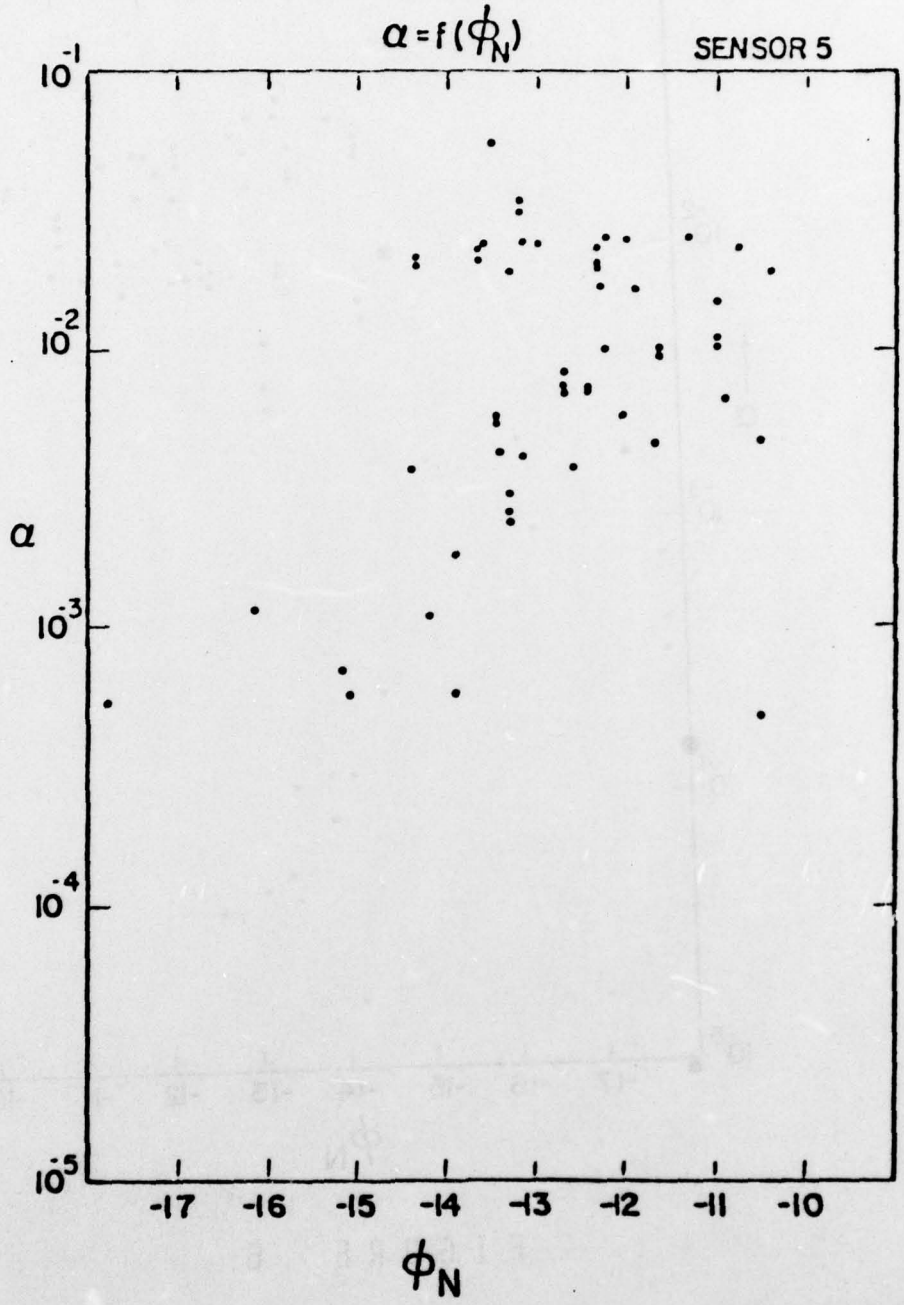

FIGURE 7

3. Discussion of Results

A. About α:

Optimally, one would seek: $\alpha = \left[\frac{I_+ (\theta=180°)}{I_+ (\theta=0°)}\right]$ rather than: $\alpha = \left[\frac{I_+ (141°<\theta<144°)}{I_+ (41°<\theta\lesssim 44°)}\right]$ as obtained from the present preliminary study. This is evidently a limitation of the present data. Other data which are now being examined show availability of measurements for: $\theta_{min} \to 0°$ and $\theta_{max} \to 180°$. In any case it should be possible to apply the appropriate sin/cos function to $I_+ (\theta_{min})$ and obtain $I_+(\theta=0°)$ but it is not possible to obtain $I_+ (\theta = 180°)$ from $I_+ (\theta \sim 144°)$. This is so since at the present time there is no reliable theoretical model for the wake zone which could unambiguously correlate the amount of depletion at θ_i with the amount of depletion at θ_k for $i \neq k$, $k > i$, or correlate unambiguously ion density ratios (for $130° \lesssim \theta \lesssim 180°$) with ion current ratios for that angular range. It is possible to use, say, a 'neutral approximation' (i.e. the approximation where ions are treated as neutral even in the very near vicinity to the satellite) and extrapolate I_+ to the maximum wake position or correlate $\left[\frac{I_+ (\theta_1)}{I_+ (\theta_2)}\right]$ with $\left[\frac{N+(\theta_1)}{N+(\theta_2)}\right]$ for θ_1 and θ_2 in the range 130°-180° but then it would be physically incorrect to use such results in a theory-experiment comparison.

B. About $\alpha = f(R_D, \phi_N)$:

The sample of data used (Orbit 1131, date: 02/24/76) has demonstrated the dependence of:

$$\alpha = \left[\frac{I_+ \text{ (wake)}}{I_+ \text{ (front)}}\right] \approx \left[\frac{I_+ \text{ (wake)}}{I_+ \text{ (ambient)}}\right] = f(R_D)$$

in the ranges:

$$24 < R_D < 56$$

$$10 < |\phi_N| < 18$$

under the limitation that $\theta_{min} \neq 0$ and $\theta_{max} \neq 180$. Namely, the amount of ion current depletion in the wake does not actually depict the situation for the maximum rarefaction zone. Nevertheless, the study already performed yielded new information not yet published. It appears from the present study that $\alpha = f(R_D)$ is more significant than a possible $\alpha = f(\phi_N)$ dependence. It should, however, be noted that such a result does not necessarily have to hold for plasmas specified by other ranges of plasma and body parameters. The continuation of the study is expected to contribute to the latter, and further explore $\alpha = f(S_{AV})$ for other flow regimes.

The results already obtained will have now to be further 'refined' and compared with other complementary results from in-situ and laboratory simulation studies as well as compared with some theoretical wake models. There is doubt whether the level of funding available to us will suffice to perform the latter. While there is doubt whether a meaningful theory-experiment study can be performed within the alloted budget, we should be able to continue the experimental investigation (via data-analysis) and extend it to be applicable and relevant to future spacelab missions.

REFERENCES

Gurevich, A.V., and Pitaevsky, L.P., "Non-linear dynamics of a rarefied ionized gas", Prog. Aerospace Sci., 16(3), p. 227, 1975.

Gurevich, A.V., Pitaevsky, L.P., and Smirnova, V.V., "Ionospheric aerodynamics", Soviet-Physics-Uspekhi, 99(1-2), p. 595, 1970.

Liu, V.C., "Ionospheric gas dynamics of satellites and diagnostic probes", Space Sci. Rev., 9, p. 423, 1969.

Liu, V.C., "On ionospheric aerodynamics", Prog. of Aerospace Sci., 16(3), p. 273, 1975.

Parker, L.W., "Computation of collisionless steady-state plasma flow past a changed disc", Report, NASA, CR-144159, 1976.

Samir, U., "Charged particle distribution in the nearest vicinity of ionispheric satellites - comparison of the main results from the Ariel I, Explorer 31 and Gemin-Agena 10 Spacecraft", in: Photon and particle interactions with surfaces in space", (ed: R.J. Grard), p. 193, 1973.

Samir, U., and Willmore, A.P., "The distribution of charged particles near a moving spacecraft", Plan. Space Sci., 13, p. 285, 1965.

Samir, U., and Willmore, A.P., "The equilibrium potential of a spacecraft in the ionosphere", Plan. Space Sci., 15, p. 1131, 1966.

Whipple, E.C., Jr., "Modeling of spacecraft charging", p. 225, in: Proc. of the Spacraft Charging Technology Conference, NASA, TMX-73537, AFGL-TR-77-0051, 1977,

Whipple, E.C., Jr., "The equilibrium electric potential of a body in the upper atmosphere and in interplanetary space", NASA-X-615-65-296, G.S.F.C., 1965.